

A quantum spin transducer based on nanoelectromechanical resonator arrays

P. Rabl^{1*}, S. J. Kolkowitz², F. H. L. Koppens², J. G. E. Harris³, P. Zoller⁴ and M. D. Lukin^{1,2}

Isolated electronic and nuclear spins in solids are at present being actively explored for potential quantum-computing applications. Spin degrees of freedom provide an excellent quantum memory, owing to their weak magnetic interactions with the environment. For the same reason, however, it is difficult to achieve controlled interactions of spins over distances larger than tens of nanometres. Here we propose a new realization of a quantum data bus for spin qubits where spins are coupled to the motion of magnetized mechanical resonators through magnetic-field gradients. Provided that the mechanical system is charged, the magnetic moments associated with spin qubits can be effectively amplified to enable a coherent spin-spin coupling over long distances through Coulomb forces. Our approach is applicable to a wide class of electronic spin qubits, which can be localized near magnetized tips and can be used for the implementation of hybrid quantum-computing architectures.

Implementation of quantum information processing faces the contradicting requirements of combining excellent isolation to avoid decoherence with the ability to control coherent interactions in a many-body quantum system. Motivated by this challenge, a wide variety of approaches have been investigated in which the quantum bits stored in long-lived states, such as those associated with spins, are mapped into other degrees of freedom to enable strong long-range couplings. This is frequently done by employing a quantum data bus that is specific to each particular qubit realization, for example mapping spin qubits to harmonic motion of trapped ions^{1–3} or photonic states associated with optically active qubits such as atoms⁴ or nitrogen-vacancy (NV) centres in diamond^{5–9}. However, such channels are absent for many spin qubits, including prominent examples such as phosphor donors in silicon^{10–13} or N@C₆₀ (refs 14–16), as well as new generations of carbon^{17,18}, and silicon^{19,20} based quantum dots.

Dramatic advances have recently been made in the fabrication and manipulation of micro- and nanoelectromechanical systems (NEMS). Examples range from applications of NEMS as nanoscale magnetometers with single-spin resolution^{21,22} to cooling of individual mechanical modes close to the quantum ground state^{23–27}. In the following we show that such NEMS can be used to create a universal quantum transducer for spin–spin interactions. In our approach, illustrated in Fig. 1a and b, spin qubits are coupled to the motion of a magnetized NEMS through magnetic-field gradients²⁸. By application of an appropriate gate voltage the mechanical system is charged and the magnetic moments associated with spin qubits are effectively amplified to enable coherent electric interactions over distances exceeding 100 μm although still being compatible with the relevant electric noise processes. The key advantages of this approach are that multiple spin set-ups can be designed and controlled using different electric-circuit layouts in a scalable architecture, the ability to couple dissimilar spins to one another and the potential to enable realization of hybrid systems in which spins are coupled to solid-state charge qubits²⁹ or isolated trapped atoms³⁰ or ions^{31,32}.

An electromechanical quantum bus for spin qubits

In what follows we discuss the implementation and operation of a spin-quantum register in which effective long range spin–spin interactions are mediated by an electromechanical quantum bus, as shown in Fig. 1c. The system consists of an array of N nanomechanical resonators each coupled magnetically to an electronic spin qubit associated with an impurity located in the substrate below. The motion of each resonator tip $i = 1, \dots, N$ along the z axis is quantized and described by the Hamiltonian $H_r^i = \hbar\omega_r a_i^\dagger a_i$ where a_i (a_i^\dagger) are annihilation (creation) operators for the fundamental vibrational mode of frequency ω_r . We model each impurity as an $S = 1/2$ electronic spin with a large frequency splitting $\omega_0 \sim$ GHz. The spin is controlled by local microwave fields of frequency ω_{mw} and described by the Hamiltonian $H_s^i(t) = \hbar(\delta_i \sigma_z^i + \Omega_i(t) \sigma_x^i)/2$, where $\sigma_{x,y,z}^i$ are Pauli operators, Ω_i is the microwave Rabi frequency and $\delta_i = \omega_0 - \omega_{mw}$. The strong magnetic-field gradients G_m produced by the magnetic tip result in a spin–resonator interaction $H_{sr}^i = \hbar\lambda/2(a_i^\dagger + a_i)\sigma_z^i$. Here $\lambda = g_s \mu_B G_m a_0/\hbar$, where $g_s \simeq 2$ and μ_B is the Bohr magneton, is the Zeeman shift associated with the zero-point motion $a_0 = \sqrt{\hbar/2m\omega_r}$ of a resonator with vibrating mass m . For a doubly clamped Si beam with dimensions $(l, w, t) \approx (25, 0.1, 0.1)$ μm and frequency $\omega_r/2\pi \sim 1$ MHz we obtain $a_0 \approx 1.6 \times 10^{-13}$ m and for gradients $G_m \approx 10^7$ T m⁻¹ (ref. 22) the resulting coupling is $\lambda/(2\pi) \approx 50$ kHz (ref. 28). Note that intrinsic spin-coherence times T_2 in the range of 1–10 ms have been observed with nitrogen-vacancy centres^{8,33} or phosphor donors¹².

To establish long-range interactions between different sites, the resonators are charged and interact capacitively with nearby wires interconnecting them. Variations of the resonator–wire capacitance $C_i(z_i)$ with the position of the tip $z_i = a_0(a_i + a_i^\dagger)$ introduce effective interactions between the resonators. For the length scales of interest, electric resonance frequencies are large compared with mechanical frequencies and the phonon–phonon coupling $\hbar g_{ij} = a_0^2 (\partial^2 W_{el}/\partial z_i \partial z_j)|_{\{z_i\}=0}$ follows from the electrostatic energy W_{el} of the underlying circuit. The resulting Hamiltonian for the

¹ITAMP, Harvard-Smithsonian Center for Astrophysics, Cambridge, Massachusetts 02138, USA, ²Department of Physics, Harvard University, Cambridge, Massachusetts 02138, USA, ³Departments of Physics and Applied Physics, Yale University, New Haven, Connecticut 06520, USA, ⁴Institute for Theoretical Physics, University of Innsbruck, and Institute for Quantum Optics and Quantum Information of the Austrian Academy of Science, 6020 Innsbruck, Austria. *e-mail: prabl@cfa.harvard.edu.

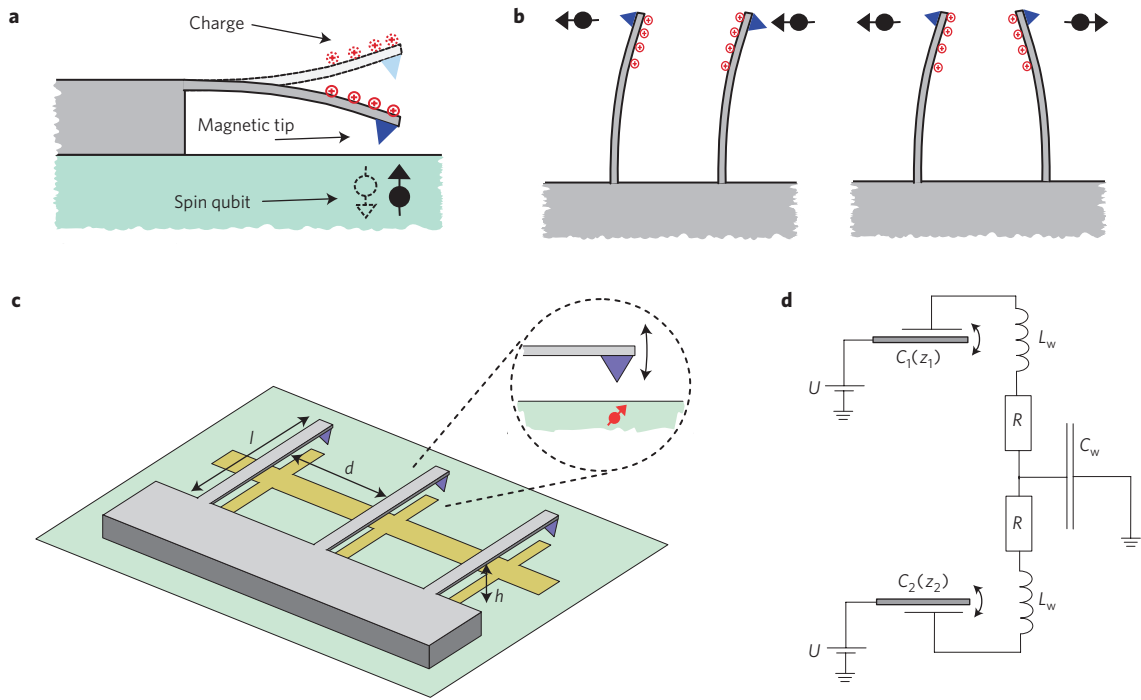


Figure 1 | Electromechanical quantum transducer. **a**, Magnetic interactions between a mechanical resonator and an electronic spin qubit lead to spin-dependent displacements of the resonator tip and convert the magnetic dipole of the spin into an electric dipole proportional to the charge on the resonator. **b**, For two resonators the difference in the electrostatic energies associated with different spin configurations then results in effective spin-spin interaction. **c**, Schematic view of a spin register based on an electromechanical quantum bus. Here resonators are coupled indirectly through capacitive interactions with nearby wires to enable coupling of spins separated by $d \sim 100 \mu\text{m}$ and to design spin-spin interactions by different circuit layouts. **d**, Circuit model that describes the coupling between two resonators.

coupled resonator array is

$$H_{\text{ph}} = \sum_i \hbar \omega_i a_i^\dagger a_i + \frac{\hbar}{2} \sum_{i,j} g_{ij} (a_i + a_i^\dagger)(a_j + a_j^\dagger) = \sum_n \hbar \omega_n a_n^\dagger a_n$$

where ω_n and $a_n = \sum_i c_{n,i} a_i$ denote frequencies and mode operators of collective phonon eigenmodes and we have absorbed a renormalization of the bare oscillation frequency into the definition of ω_i . To estimate the typical coupling strength we consider two sites separated by a distance d and connected by a wire of self-capacitance $C_w \approx \epsilon_0 d$, where ϵ_0 is the vacuum permittivity. Then, as shown in Fig. 1d, $W_{\text{el}} = -(U^2/2)(C_\Sigma C_w / C_\Sigma + C_w)$, where $C_\Sigma = C_1(z_1) + C_2(z_2)$ and U is the applied voltage. Assuming $C_i(z_i) \simeq C(1 - z_i/h)$, where h is the mean electrode spacing, we obtain for $g \equiv g_{12}$

$$\hbar g = \frac{C^2 C_w^2 U^2}{(2C + C_w)^3} \frac{a_0^2}{h^2}$$

For two resonators separated by $d = 100 \mu\text{m}$ and with dimensions given above, $h \approx 100 \text{nm}$ and a typical electrode capacitance $C \approx 0.1 \text{fF}$, we obtain $g/(2\pi) \approx 25 \text{kHz}$ for $U = 1 \text{V}$. Voltages up to $U \approx 10 \text{V}$ (ref. 23) can lead to phonon-phonon interactions as large as 1MHz .

After combining magnetic and electric interactions we obtain the full spin-register Hamiltonian $H = \sum_i H_s^i + \sum_i H_{\text{sr}}^i + H_{\text{ph}}$, which by setting $\lambda_{n,i} = \lambda c_{n,i}$ is

$$H = H_s(t) + \sum_n \omega_n a_n^\dagger a_n + \frac{1}{2} \sum_{i,n} \lambda_{i,n} (a_n^\dagger + a_n) \sigma_z^i \quad (1)$$

This model of spins coupled to a set of collective phonon modes is familiar from quantum-computing proposals with trapped ions^{1,34–38}, and in principle similar gate schemes as developed in this field can be applied for spin-entangling operations here.

However, the physical realization is quite different, and in particular decoherence processes in the form of mechanical dissipation and electric-field noise must be addressed. In the following we therefore describe the implementation of gate operations based on off-resonant spin-phonon interactions^{34–38} that are consistent with spin-echo techniques to eliminate low-frequency noise and avoid ground-state cooling requirements. Alternatively, gate operations based on a resonant exchange of phonons¹ could be implemented using techniques described in ref. 28.

Spin-spin interactions

For the following discussion it is convenient to change to a displaced oscillator basis that is related to the uncoupled basis by a polar transformation $U = e^{-iS}$, where $S = (1/2) \sum_i P_i \sigma_z^i$ and $P_i = i \sum_n \lambda_{n,i} / \omega_n (a_n^\dagger - a_n)$ are collective momentum operators. In this new representation and for $\delta_i = 0$ the resulting spin-register Hamiltonian, $H \rightarrow U H U^\dagger$, is^{36,39}

$$H = \sum_i \frac{\hbar \Omega_i(t)}{2} (\sigma_+^i e^{-iP_i} + \sigma_-^i e^{iP_i}) - \hbar \sum_{i \neq j} M_{ij} \sigma_z^i \sigma_z^j + H_{\text{ph}} \quad (2)$$

Let us for the moment assume that $\Omega_i(t) = 0$ where equation (2) reduces to an ‘always on’ Ising interaction with coupling strength $M_{ij} = \sum_n \lambda_{n,i} \lambda_{n,j} / (4\omega_n)$, which is mediated by but independent of phonon modes. The origin of this interaction can be understood from spin-dependent displacements of the resonators’ equilibrium positions as described in Fig. 2a. The evolution under Hamiltonian (2) then results in a spin-entangling operation

$$U_g(t_g) = e^{i(\sum_{i,j} M_{ij} \sigma_z^i \sigma_z^j) t_g} \quad (3)$$

For $N = 2$ an initially separable spin-superposition state, for example, $|\psi\rangle_0 = \prod_{i=1,2} (|0_i\rangle + |1_i\rangle) / \sqrt{2}$ evolves into an entangled state $|\psi\rangle(t_g) = (|00\rangle + |11\rangle + i|01\rangle + i|10\rangle) / 2$ on a timescale

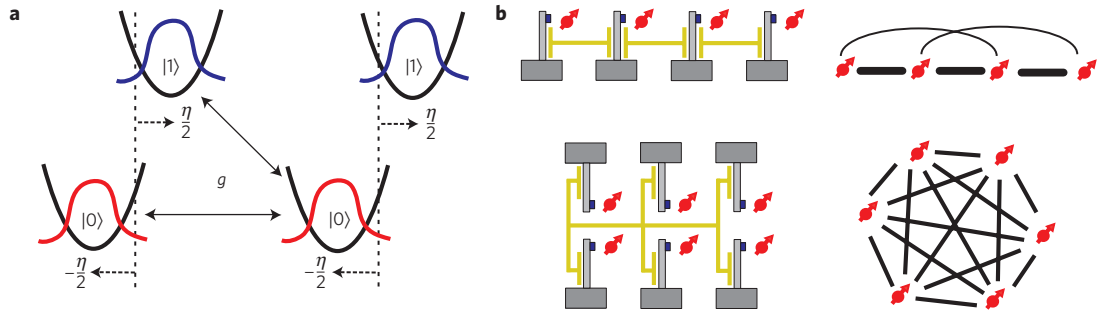


Figure 2 | Spin-spin interactions. **a**, In the ‘displaced oscillator basis’ different spin states $|0\rangle, |1\rangle$ are associated with different resonator equilibrium positions displaced in phase space by an amplitude $\pm\eta/2$. Consequently, electric interactions between the resonators, $g \neq 0$, translate into Ising interactions $\sim \sigma_z^1 \sigma_z^2$ with a strength proportional to η^2 . **b**, Two basic examples for different circuit layouts (left) and the corresponding effective Ising interactions (right), where the coupling strength $|M_{ij}|$ is indicated by the thickness of the lines.

$t_g = \pi/(8|M|)$. Here $M = \eta^2 \omega_r (1/\xi - 1)/8$ is the characteristic interaction strength, $\eta = \lambda/\omega_r$ is the magnetic coupling parameter and $\xi = \omega_0/\omega_1$ the ratio between the two phonon frequencies, where $\xi (g \ll \omega_r) \simeq 1 + 2g/\omega_r$ and $\xi (g \gg \omega_r) \simeq 2\sqrt{g}/\omega_r$. We see that the gate speed is optimized under strong-coupling conditions $\lambda, g \gtrsim \omega_r$, that is, when the spin displaces the resonator by more than its zero-point motion. In principle, this condition can always be achieved by choosing a resonator with smaller vibration frequency ω_r , but practical limitations can prevent this as discussed below.

For $N > 2$ the coupling matrix M_{ij} depends on the phonon properties and therefore on the layout of the underlying electric circuit (Fig. 2b). This property offers a simple way to design and control different types of multi-spin interaction. For example, connecting neighbouring resonators by individually isolated wires results in a nearest-neighbour phonon coupling $g_{i,i+1} = g$ and a spectrum $\omega_n = \sqrt{\omega_r^2 + 4\omega_r g(1 + \cos((n+1)\pi/N))}$. For $g \ll \omega_r$ we find that $M_{i,i\pm 1} \simeq \eta^2 g/4$, and interactions quickly decay as $M_{i,i\pm m} \sim (g/\omega_r)^{(m-1)}$ for larger spin separations. Hamiltonian (2) then corresponds to an Ising model with nearest-neighbour coupling M and extensions to a two-dimensional lattice are discussed below. In contrast, by coupling all resonators to a single wire we obtain $g_{ij} = g/(N-1)$ and the phonon spectrum consists of only two frequencies: $\omega_0 = \sqrt{\omega_r^2 + 2\omega_r gN/(N-1)}$ is the frequency of the centre-of-mass mode with $c_{0,i} = 1/\sqrt{N}$, whereas all other orthogonal modes are unaffected and $\omega_{n>0} = \omega_r$. This configuration translates into an ‘infinite range’ or collective spin model $H \simeq \hbar M S_z^2$, where $S_z = \sum_i \sigma_z^i / \sqrt{N}$, applicable for the generation of spin-squeezed⁴⁰ or highly entangled N -particle Greenberger–Horne–Zeilinger states³⁵. Generally, we see that the NEMS array maps a given electric circuit onto a corresponding Ising model H_{Ising} , and thereby also maps the flexibility of electric circuit layouts onto an equivalent flexibility in the design of spin–spin interactions.

Decoherence and spin echo

Our analysis of spin–spin interactions so far has ignored the presence of various decoherence processes that degrade the implementation of quantum gate operations in a realistic setting. In particular, we must address the effect of mechanical dissipation and—as the resonators are charged—that of Johnson–Nyquist and other electric noise sources on the coherence of the mechanical quantum bus. Before we discuss the influence of decoherence on gate operations, we remark that dephasing of an idle qubit is eliminated to a large extent by encoding quantum information in nuclear-spin states located in the vicinity of the electronic spin. Prolonged storage times and gate operations between nuclear and electronic spins on a 10–100 ns timescale have already been demonstrated in several experiments^{6,9,11,16}. This approach enables us to use swap operations between nuclear and electronic spins to switch on and off Ising interactions—together with all related

dephasing processes—only for a specific set of qubits and for a specified time. In a scenario where each electronic spin is coupled to several nuclear spins, we might in addition benefit from entanglement purification schemes^{41,42}, relaxing the bounds on tolerable errors in each individual gate operation.

For the duration of a gate operation, quantum information is encoded in electronic spin superposition states and leads to a loss of coherence $\sim e^{-(t_g/T_2)^\alpha}$ due to interactions of the spins with their local magnetic environment. Here $\alpha \geq 1$ depends on specific properties of the environment and details of the actual gate sequence^{43–45}. In addition, as shown in Fig. 2a, each spin superposition in the displaced oscillator basis also corresponds to a motional ‘Schrödinger cat’ state, which is affected both by mechanical as well as electric noise. In the Methods section we detail a model for motional decoherence processes and derive general expressions for the resulting gate fidelities. As the essential result, we find that for the case of two coupled spins the fidelity of a single entanglement operation decreases as

$$F \simeq 1 - R(\xi) \frac{\Gamma_r}{\omega_r} - \left(\tau(\xi) \frac{\omega_r}{\lambda^2 T_2} \right)^\alpha \quad (4)$$

The first term describes motional decoherence where $R(\xi) = 3\pi(\xi + \xi^{-1})/2(\xi - 1)$ and $\Gamma_r = \Gamma_m + \Gamma_{\text{el}}$ is the sum of the mechanical and electrical decoherence rates. For a support temperature T and a mechanical quality factor Q_m we obtain $\Gamma_m = k_B T / \hbar Q_m$, and $\Gamma_{\text{el}} \approx a_0^2 C^2 U^2 S_E(\omega_r) / \hbar^2$ for a given electric-field fluctuation spectrum $S_E(\omega) = \text{Re} \int_0^\infty d\tau \langle E(\tau)E(0) + E(0)E(\tau) \rangle e^{-i\omega\tau}$. The second term in equation (4) describes the effect of bare spin dephasing mentioned above, where $\tau(\xi) = t_g/(\omega_r/\eta^2) = \pi\xi/(\xi - 1)$ can be identified with the normalized gate time.

Equation (4) shows that for ideal spin qubits the gate fidelity is independent of λ . This can be understood from the fact that both the effective spin–spin coupling and the dephasing rate of a motional superposition state scale with the square of the displacement amplitude $\eta = \lambda/\omega_r$. For $\omega_r \gg g$ we obtain $R(\xi) \approx 3\pi\omega_r/2g$ and the fidelity is limited by the ratio Γ_r/g , meaning that strong-coupling conditions are required only with respect to electric interactions. However, the overall gate time $t_g \sim \eta^{-2}$ increases for small η , and for a finite spin dephasing time T_2 there is a competition between spin and motional decoherence processes. Then, for a fixed λ and under the assumption that $g \gtrsim \omega_r$ is satisfied, there exists an optimal frequency ω_r^{opt} for which gate errors scale as $\sim (\Gamma_r/\lambda^2 T_2)^\alpha/(\alpha+1)$ and high gate fidelities can be achieved for either small spin or motional dephasing times. In Fig. 3 we plot the optimized gate fidelity as a function of Γ_r and T_2 .

At $T = 100$ mK a mechanical quality factor of $Q_m \sim 10^6$ corresponds to $\Gamma_m/2\pi \simeq 2$ kHz, and for the parameters $\omega_r/2\pi = 1$ MHz, $\lambda/2\pi = 50$ kHz and $g/2\pi \simeq 500$ kHz gate fidelities close to $F \approx 0.99$ can be achieved with realistic spin

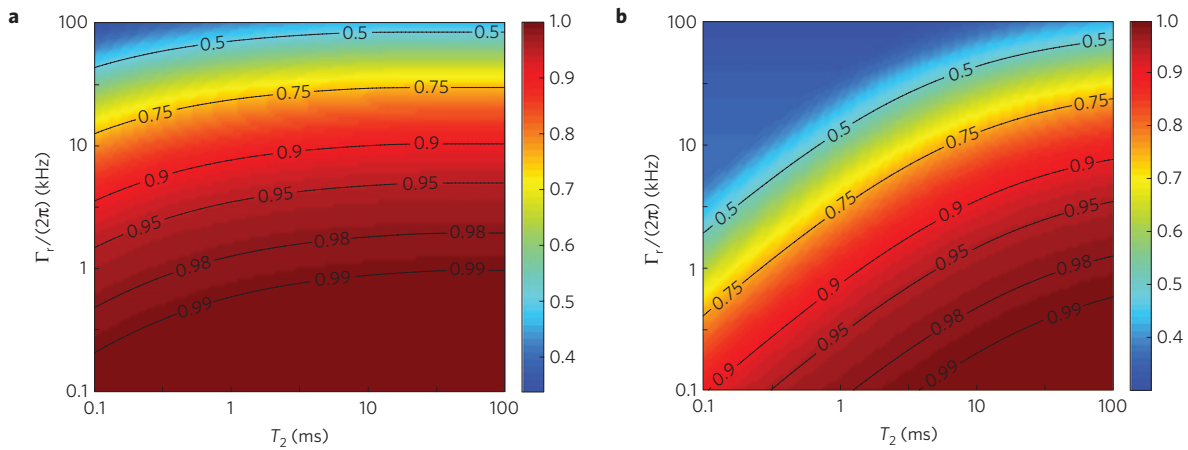


Figure 3 | Gate fidelity. **a, b**, The fidelity F of a two-qubit operation discussed in equation (4) is plotted as a function of the motional decoherence rate Γ_r and the spin coherence time T_2 assuming $\alpha = 3$. The magnetic coupling strength is $\lambda/2\pi = 100$ kHz (**a**) and $\lambda/2\pi = 10$ kHz (**b**). In both plots $g/2\pi = 500$ kHz and the resonator frequency $\omega_r/2\pi$ is optimized within the interval from 1 kHz to 5 MHz. The linear increase of the lines of constant fidelity indicates a scaling of gate errors as $\sim(\Gamma_r/\lambda^2 T)^{3/4}$, and for increasing T_2 the fidelity is limited by motional dephasing, $1 - F \sim \Gamma_r/g$.

coherence times $T_2 \approx 10$ ms. Note that in combination with entanglement purification schemes^{41,42} fidelities of $F > 2/3$ are in principle sufficient, which would relax some of the experimental requirements and makes this technique applicable for temperatures up to $T \sim 1$ K.

For $C_w \gg C$ the influence of electric noise can be expressed as $\Gamma_{el}/g \approx C_w S_V(\omega_r)/\hbar$, where $S_V(\omega) := h^2 \times S_E(\omega)$. Johnson–Nyquist noise from a resistor R leads to voltage fluctuations $S_V(\omega) = 4k_B T R$. For a 200-nm-thick and $d \approx 100$ - μ m-long gold wire $R \sim 1 \Omega$, and for $C_w = 1$ fF, $T = 100$ mK we obtain $\Gamma_{el}/g \approx 5 \times 10^{-5}$. In addition, we must consider the effect of ubiquitous $1/f$ noise, which we model by a spectrum $S_V(\omega) = (z_c/l) A_V/\omega$ (Supplementary Information). Here $z_c < l$ is the noise correlation length, which we approximate by the distance between the resonator and the substrate, $z_c \sim 0.1$ – 1μ m. Typical values for $A_V = 10^{-12}$ – $10^{-14} V^2$ can be estimated from charge noise measurements⁴⁶ and are consistent with strong-coupling requirements $\Gamma_{el}/g \sim 0.001$ – 0.1 .

The spin coupling described by equation (2) relies on a static displacement of the mechanical resonators and therefore gate operations are in principle also affected by the low-frequency part of the magnetic- and electric-noise spectrum. It is known that for single spins low-frequency noise can be cancelled out efficiently using spin-echo techniques^{47,48} where gate operations are interrupted by a sequence of fast π rotations. Here the spin–spin interactions $\sim \sigma_z^i \sigma_z^j$ are invariant under simultaneous rotations of both spins and therefore the gate operations discussed above are compatible with such techniques. However, as illustrated in Fig. 4a, any rotation of the spin, which includes the initial preparation step, is also accompanied by a displacement of the resonator modes and thereby entangles spin and motional degrees of freedom. Specifically, a total gate sequence with N_p echo pulses applied at times $t_{p=1, \dots, N_p}$ will excite each phonon mode by a spin-dependent amplitude proportional to $\beta(\omega_n) = 1/2(1 - e^{i\omega_n t_g}) + \sum_{p=1}^{N_p} (-1)^p e^{i\omega_n t_p}$. Therefore, as illustrated in Fig. 4b, the basic strategy for avoiding enhanced motional dephasing is to identify a sequence of pulses satisfying $\beta(\omega_n) = 0, \forall n$. In the Methods section we show that under these conditions dephasing from magnetic and electric low-frequency noise is strongly suppressed and the resulting gate fidelity is described by equation (4) but with modified parameters $R(\xi)$ and $\tau(\xi)$. In Fig. 4c and d those parameters are plotted for a specific set of pulse sequences.

Under realistic conditions pulse errors result in a finite excitation and decrease the fidelity by a factor $\sim e^{-2\eta^2(2N_i+1)\Delta\beta^2}$. Here $\Delta\beta^2 = (1/N) \sum_n (\omega_r/\omega_n)^3 |\beta(\omega_n)|^2$ and N_i is the initial occupation

number of the resonator mode, which can be made much lower than the thermal occupation number N_{th} by actively cooling the resonator in between the gate operations. Therefore, moderate cooling to $N_i \sim 10$ – 100 (refs 23–28) already makes the gate robust against technical imperfections, although still enabling coupling parameters in the range of $\eta \sim 0.1$ – 1 .

In summary, our analysis shows that the proposed coupling scheme is compatible with the main decoherence processes in the form of mechanical dissipation, Johnson–Nyquist noise and the ubiquitous electric $1/f$ noise encountered in solid-state systems. In addition, the coupling scheme can be combined with spin-echo techniques to make it robust also against other low-frequency noise sources. For a specific experimental setting, further improvements can be expected from more advanced spin-echo schemes⁴⁸ and numerical pulse-optimization methods³⁸.

Quantum computing and scalability

We finally discuss potential realizations of scalable quantum-computing architectures that are based on NEMS-mediated spin–spin interactions. Let us first consider a small subunit of N_s resonators coupled by a single wire. In this case the phonon spectrum is independent of N_s and the pulse sequences discussed above directly apply for any multiqubit gate. For state preparation and detection we distinguish between at least one ‘control’ and the remaining ‘passive’ qubits. For the control qubit we choose, for example, a nitrogen-vacancy centre, which can be polarized and detected optically. Two qubit gates are used to carry out a mapping $|0\rangle_c(\alpha|0\rangle_i + \beta|1\rangle_i) \rightarrow (\alpha|0\rangle_c|0\rangle_i + \beta|1\rangle_c|1\rangle_i)$ such that a successive detection of the control spin implements a quantum non-demolition measurement of the state of the i th spin. For state preparation the known spin state is rotated afterwards to the desired target state using local operations. By this approach the ‘passive’ spins can be optimized with respect to their coherence properties, optical detection is spatially separated from storage qubits and optical pumping of the control spin can be employed to cool the phonon modes between gate operations²⁸. However, the scaling of Ising interactions $\sim 1/N_s$ limits the size of a single subregister to a few or, including several electronic/nuclear spins per resonator, to a few tens of qubits. To go beyond this limit individual subregisters can be connected by a switchable coupling as described in Fig. 5a. Although the mode spectrum of two coupled registers is slightly more complicated (for example, five different frequencies), the operation of a large-scale quantum computer can still be reduced to gate operations within one or at most two subregisters.

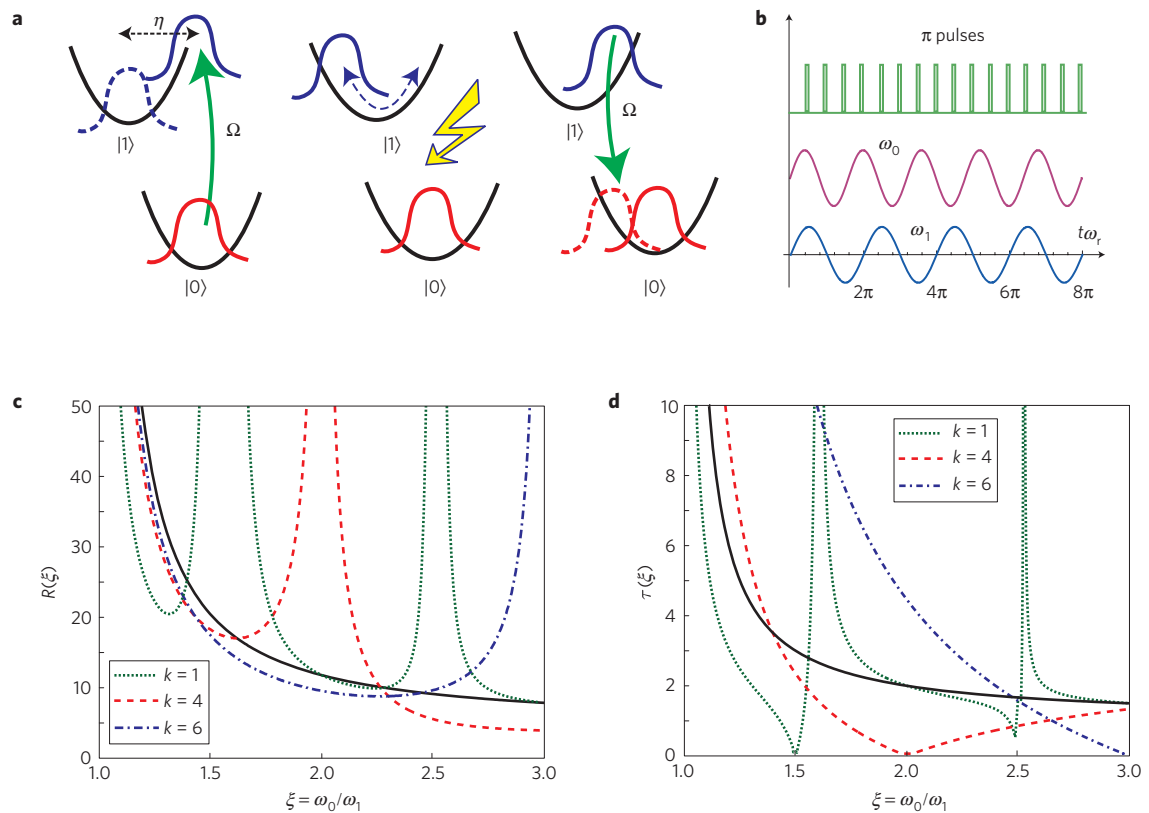


Figure 4 | Spin-echo techniques. **a**, A fast flip of the spin state is accompanied by a displacement of the resonator state by $\pm\eta$ relative to its equilibrium position and entangles spin and motional degrees of freedom. Dephasing of motional superposition states during the gate and a non-vanishing excitation of the phonon modes at the end of the gate sequence reduce the gate fidelity. **b**, Example for a spin-echo sequence with $N_p = nk$ fast π pulses applied at times $\omega_r t_p = p \times 2\pi/k$, where n and k are integers. To achieve $\beta(\omega_{0,1}) = 0$ the pulses are chosen to be commensurate with the phonon frequencies, which here is shown for $k = 4$ π pulses per cycle and a frequency ratio $\xi = \omega_0/\omega_r = 5/4$. **c**, Effective motional decoherence parameter $R(\xi)$ for spin-echo sequences with $k = 1, 4, 6$ pulses per oscillation period. **d**, The normalized gate time $\tau(\xi)$ for the same conditions. In both plots the solid line indicates the analytic result used in the discussion of equation (4), which away from individual resonances captures the overall behaviour well.

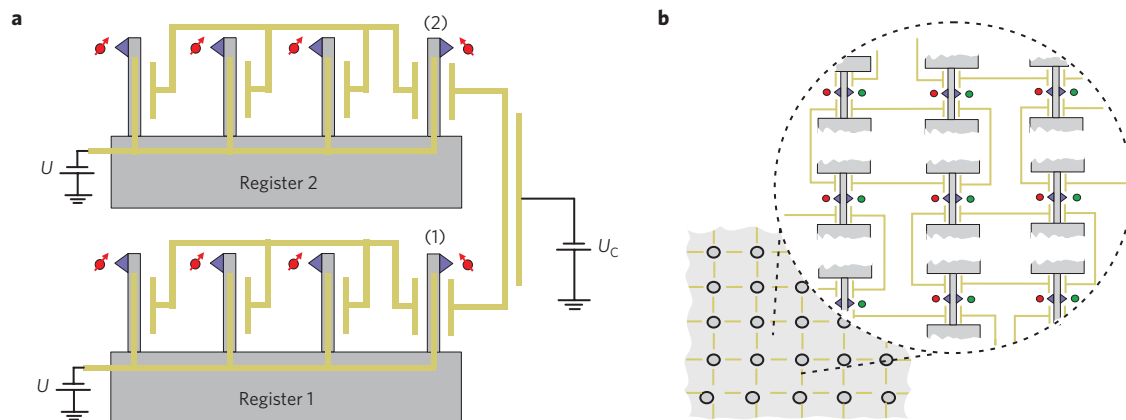


Figure 5 | Scalable quantum information processing. **a**, Implementation of a switchable coupling between two subregisters. For a control voltage $U_c = 0$ a finite electric coupling $g_{12} \approx g$ between resonators 1 and 2 enables gate operations between spins located in different registers. For $U_c \approx U$ there is no energy associated with charge flowing from the gate capacitors onto the wire and thereby the coupling $g_{12} \approx 0$ is switched off. **b**, A scalable quantum-computing architecture, based on the concept of one-way quantum computing⁴⁹. Resonators are ordered on a two-dimensional lattice and coupled to their four neighbours electrostatically. This configuration results in an effective spin Hamiltonian $H \approx \hbar M \sum_{(i,j)} \sigma_z^i \sigma_z^j$, which can be used to generate cluster states as an entanglement resource. With each node consisting of multiple spins, the cluster state can be stored in long-lived electronic or nuclear spin qubits (green dots), and local measurements, the actual computation step in one-way quantum computing, can be carried out through an optically active spin (red dots), for example, a nitrogen-vacancy centre.

An alternative approach is sketched in Fig. 5b, where the resonators are ordered in a two-dimensional lattice structure with nearest-neighbour coupling. This layout is motivated by the

concept of one-way quantum computing⁴⁹, where in a first step a cluster state is prepared as an entanglement resource whereas the actual computation is done by measurements and local spin

operations only. The cluster state is generated by applying the gate operation U_g given in equation (3) consecutively or in parallel to each spin i and its four nearest neighbours. The nearest-neighbour coupling $M_{i,i+1} \simeq \eta^2 g/4$ is independent of the lattice size, and as interactions decay quickly with distance many gates can be carried out in parallel. However, for a large lattice the phonon spectrum is almost continuous, the condition $\beta(\omega_n) = 0$ can no longer be strictly fulfilled and $\Delta\beta > 0$. A numerical evaluation of $\Delta\beta$ for $g/\omega_r = 0.2$ and a $k = 4$ spin-echo sequence commensurate with $\max\{\omega_n\}$ gives $\Delta\beta^2 \sim 0.015$, roughly independent of the length of the gate sequence. For $\eta^2 N_i < 1$ the resulting error of $\sim 1\%$ is still sufficiently low.

Conclusions and outlook

In summary, we have proposed the application of NEMS as a universal quantum transducer for spin–spin interactions. Compared with direct magnetic coupling or probabilistic optical entanglement schemes, our approach enables the implementation of long-range and deterministic spin-entanglement operations as well as the design and control of multispin interactions by simple electric circuitry. The universality of the basic underlying concept, namely to use the mechanical resonator for a coherent conversion of magnetic into electric dipoles, also opens a wide range of possibilities for the integration of electronic and nuclear spins with other charge-based quantum systems. Specifically, it might be interesting to consider hybrid architectures by coupling spins with transmission-line cavities²⁷, charge qubits²⁹ and trapped ions^{31,32} or atoms³⁰. Moreover, this technique can be applicable for a remote magnetic sensing of ‘dark’ spins in a condensed-matter or biological environment that is incompatible with direct laser illumination. In a broader perspective, the quantum transducer ability of NEMS can therefore be seen as one of the fundamental applications of ‘quantum’-mechanical systems.

Methods

To evaluate the effect of motional decoherence on gate operations we consider a model described by a total Hamiltonian

$$H_{\text{tot}} = H + \sum_{n,k} \frac{\hbar g_k}{2} (a_n + a_n^\dagger) (b_{n,k} + b_{n,k}^\dagger) + \hbar \omega_k b_{n,k}^\dagger b_{n,k}$$

Here H is the system operator (1), $b_{n,k}$ ($b_{n,k}^\dagger$) are bosonic annihilation (creation) operators for the modes of the bath with $[b_{n,k}, b_{n',k'}^\dagger] = \delta_{nn'} \delta_{kk'}$ and g_k is the coupling between the resonators and the k th bath mode. The environment is characterized by the spectral density $J(\omega) = (\pi/2) \sum_k g_k^2 \delta(\omega - \omega_k)$ (ref. 39), which we assume to be equal for all modes. In thermal equilibrium $J(\omega)$ is related to the force fluctuation spectrum by $S_F(\omega) = \hbar^2 J(\omega) \coth(\hbar\omega/2k_B T)/2a_0^2$ (Supplementary Information). Clamping losses and Johnson–Nyquist noise can be described by a purely ohmic environment with $J(\omega) = \omega/Q$, whereas the effect of (non-equilibrium) $1/f$ noise can be taken into account by setting $J(\omega) \coth(\hbar\omega/2k_B T) = \text{constant} \times \omega^{-1}$. Below we identify $\Gamma_r := a_0^2 S_F(\omega_r)/\hbar^2$ as the relevant decoherence rate.

To include spin-echo techniques we assume that in the limit of fast π pulses the bare evolution of the spin operators reduces to $\sigma_z^i(t) = f(t)\sigma_z^i$. Here $f(t) = 2 \sum_{p=0}^{N_g-1} z_p \theta(t - t_p)$, $\theta(t)$ is the unit step function, $z_0 = -z_{N_g-1} = 1/2$ and $z_p = (-1)^p$ otherwise. $f(t)$ describes the effect of alternating spin flips at times t_p and the first and last terms account for the initial and final spin preparation steps at $t_0 = 0$ and $t_{N_g+1} = t_g$. The total Hamiltonian can then be written as

$$H_{\text{tot}} = H_{\text{osc}} + \frac{\hbar \lambda}{2} \sum_n f(t) x_n S_z^n \quad (5)$$

where $S_z^n = \sum_i c_{n,i} \sigma_z^i$, $x_n = (a_n + a_n^\dagger)$ and H_{osc} is the Hamiltonian of the coupled resonator and bath degrees of freedom. The evolution generated by Hamiltonian (5) is

$$U_g(t_g) = \prod_{n=1}^N e^{-i \frac{\lambda}{2} \int_0^{t_g} ds f(s) x_n S_z^n} e^{i \Phi_n(S_z^n)}$$

where $x_n(t) = e^{iH_{\text{osc}}t/\hbar} x_n e^{-iH_{\text{osc}}t/\hbar}$ and the geometric phases Φ_n are given by

$$\Phi_n = i \frac{\lambda^2}{8} \int_0^{t_g} ds \int_0^s ds' f(s) f(s') [x_n(s), x_n(s')]$$

For a given initial pure spin state $|\psi_0\rangle$ and a target state $|\psi_f\rangle = \prod_n e^{i\Phi_n(S_z^n)} |\psi_0\rangle$, we define the gate fidelity as $F = \text{Tr}\langle\psi_f| U_g |\psi_0\rangle \langle\psi_0| \otimes \rho_{\text{osc}}(0) U_g^\dagger |\psi_f\rangle$, where

$\rho_{\text{osc}}(0)$ is the initial state of the oscillator modes. We here assume pure dephasing processes only and write $|\psi_0\rangle = \sum_s c_s |s\rangle$ where $\sigma_z^i |s_i\rangle = s_i |s_i\rangle$. Then, by setting $s_n = \sum_i c_{n,i} s_i$ the fidelity can be written as

$$F = \sum_{s,r} |c_s|^2 |c_r|^2 e^{-\frac{\lambda}{2} \sum_n F_n(t_g) (s_n - r_n)^2}$$

The decoherence functionals are in general defined as

$$F_n(t_g) = \frac{\lambda^2}{4} \int_0^{t_g} ds \int_0^s ds' f(s) f(s') \langle \{x_n(s), x_n(s')\} \rangle_0$$

where $\langle \cdot \rangle_0$ denotes the average over the initial state $\rho_{\text{osc}}(0)$ and $\{ \cdot \}$ is the anticommutator.

Equilibrium. When the resonator modes are in thermal equilibrium with the environment, $\rho_{\text{osc}}(0) = \prod_{n,k} \rho_{n,k}$, we can re-express $x_n(t)$ in terms of eigenoperators $d_{n,k}$ and eigenfrequencies $\omega_{n,k}$ of the coupled oscillator Hamiltonian H_{osc} , that is, $\lambda x_n(t) = \sum_k \lambda_{n,k} (d_{n,k}^\dagger e^{i\omega_{n,k}t} + d_{n,k} e^{-i\omega_{n,k}t})$. For $\eta_n = \lambda/\omega_n$ we introduce an effective spectral density $J_{\text{eff}}^n(\omega) := (\pi/2\eta_n^2) \sum_k \lambda_{n,k}^2 \delta(\omega - \omega_{n,k})$, which can be interpreted as the environmental noise filtered by the mechanical response of the resonator. It can be expressed in terms of $J(\omega)$ by the relation $J_{\text{eff}}^n(\omega) = J(\omega)\omega_n^4 / [(\omega_n^2 - \omega^2)^2 + \omega_n^2 \Gamma^2(\omega)]$ (ref. 50). For $Q \gg 1$ it is strongly peaked around $\omega \approx \omega_n$ and for the geometric phases we obtain

$$\Phi_n(t_g) \simeq \eta_n^2 \left[\frac{t_g}{4\omega_n} + \frac{1}{\omega_n^2} \sum_{p=1}^{N_r+1} \sum_{p'=0}^{p-1} z_p z_{p'} \sin(\omega_n(t_p - t_{p'})) \right] \quad (6)$$

with additional corrections $\sim O(t_g \omega_r / Q)$. The first term represents the bare Ising interactions, $\Phi_n(t_g) = \eta_n^2 \omega_n t_g / 4$, whereas the second term in equation (6) describes additional geometric phases, which depend on the spin-echo pulse sequence. For the coherence functionals we obtain the general expression

$$F_n = \frac{4\eta_n^2}{\pi} \int_0^\infty d\omega \frac{J_{\text{eff}}^n(\omega)}{\omega^2} \coth\left(\frac{\hbar\omega}{2k_B T}\right) |\beta(\omega)|^2 \quad (7)$$

where $|\beta(\omega)|^2 = \sin^2(\omega t_g/2)$ for a gate without spin echo and $|\beta(\omega)|^2 = \sin^2(n\pi\omega/\omega_r) \tan^2(\pi\omega/(k\omega_r))$ for k equidistant spin-echo pulses per oscillation period $2\pi/\omega_r$. Equation (7) is familiar from discussion of spin dephasing within the spin-boson model (see for example refs 39,48), but here qualitatively different results emerge from the resonant structure of $J_{\text{eff}}^n(\omega)$. For isolated resonator modes with a thermal occupation number $N_{\text{th}}^{(n)}$, equation (7) reduces to $F_n \simeq 4\eta_n^2 N_{\text{th}}^{(n)} |\beta(\omega_n)|^2$ as a result of the residual entanglement between spins and the bare resonator modes at the end of the gate sequence. For the low-frequency part of the integral in equation (7), F_n , we can approximate $J_{\text{eff}}^n(\omega \ll \omega_n) \approx J(\omega)$, and without spin echo we obtain $F_n \simeq 2\eta_n^2 \Gamma_r t_g$ for ohmic noise whereas it diverges for $1/f$ noise. However, including spin echo we find that $\lim_{\omega \rightarrow 0} J(\omega) |\beta(\omega)|^2 / \omega^3 = 0$ for both ohmic and $1/f$ noise, and in the latter case the low-frequency part F_n grows only logarithmically with t_g . The main contribution to F_n then comes from near-resonant modes $\omega \approx \omega_n$ characterized by the rate Γ_r .

To be more specific, we consider the case of $N = 2$ and a symmetric initial state with $c_s = 1/4$. We define an effective interaction strength $M_{\text{eff}} = (\Phi_0(t_g) - \Phi_1(t_g))/t_g$ and introduce an average motional dephasing rate $\Gamma_{\text{eff}} = (F_0 + F_1)/(2t_g)$. In the limit of high fidelities we obtain $F \simeq 1 - \pi \Gamma_{\text{eff}} (4M_{\text{eff}} - F_s(t_g) - F_r(t_g))$, where we have added the bare spin dephasing contribution $F_s(t_g) \simeq (t_g/T_2)^q$. With the definition $R(\xi) := \pi\omega_r \Gamma_{\text{eff}} / (4M_{\text{eff}} \Gamma_r)$ and $\tau(\xi) = \pi\eta^2 \omega_r / 4M_{\text{eff}}$, we obtain the general form of F given in equation (4), where the analytic expressions for $R(\xi)$ and $\tau(\xi)$ have been derived for an ohmic bath and without spin echo.

Non-equilibrium. If the phonon modes are precooled to a temperature $T_i \ll T$ the initial density operator $\rho_{\text{osc}}(0) = \prod_n \rho_n(T_i) \prod_k \rho_{n,k}(T)$ is diagonal in the uncoupled resonator and bath operators. In this case we calculate the time evolution for the phonon mode operators $x_n(t)$, which for $t\omega_r \gg 1$ obey the equation of motion,

$$\ddot{x}_n(t) + \gamma_n \dot{x}_n(t) + \omega_n^2 x_n(t) = -\omega_n \sum_k g_k (b_{n,k}^\dagger e^{i\omega_k t} + b_{n,k} e^{-i\omega_k t}) \quad (8)$$

where $\gamma_n = \omega_n/Q$. The solutions of equation (8) can be divided into terms containing system and bath operators only, $x_n(t) = x_n^{(s)}(t) + x_n^{(b)}(t)$, and accordingly we decompose $F_n = F_n^{(s)} + F_n^{(b)}$. For a weakly damped resonator we obtain $x_n^{(s)}(t) \simeq (x_n \cos(\omega_n t) + p_n \sin(\omega_n t)) e^{-\gamma_n t/2}$ and $F_n^{(s)} \simeq 2\eta_n^2 (2N_i + 1) |\beta(\omega_n + i\gamma_n/2)|^2$, where N_i is the initial occupation number. The contribution from the bath is

$$x_n^{(b)}(t) = -\omega_n \sum_k g_k (v_n(\omega_k, t) b_{n,k}^\dagger + v_n^*(\omega_k, t) b_{n,k})$$

where $v_n(\omega, t) = L^{-1}[(s^2 + \gamma s + \omega_n^2)^{-1} (s - i\omega)^{-1}]$ and L^{-1} denotes the inverse Laplace transformation. For low frequencies, $\omega_k < \omega_r$, we approximate $v_n(\omega, t) \approx e^{i\omega t} / \omega_n^2$, and in this regime we recover the same result as given

in equation (7) for the equilibrium case. For near-resonant modes we use $v_n(\omega, t) \approx (e^{i\omega t} - e^{i(\omega_n - \gamma_n/2)t}) / (\omega_n(2(\omega_n - \omega) + i\gamma_n))$ and obtain

$$F_n^{(b)} \simeq F_n^l + \eta_n^2 N_{\text{th}}^{(n)} \frac{2}{\pi} \int_{-\infty}^{\infty} d\omega \frac{\gamma_n |\beta(\omega_n + i\gamma_n/2) - \beta(\omega)|^2}{(\omega - \omega_n)^2 + \gamma_n^2/4}$$

Evaluating this integral we find in summary that for $N_i \ll N_{\text{th}}^{(n)}$ and $\gamma_n t_g \ll 1$ the motional decoherence coefficients are

$$F_n \simeq F_n^l + 4\eta_n^2 \left[\left(N_i + 1/2 \right) |\beta(\omega_n)|^2 + \Gamma_m \sum_{p,p'} z_p z_{p'} e^{i\omega_n(t_p - t_{p'})} |t_p - t_{p'}| \right]$$

We see that to first order in $\gamma_n t_g$ the effect of pulse errors, $\beta(\omega_n) \neq 0$, scales only with the initial occupation number N_i whereas low-frequency noise and interactions with near-resonant environmental modes leads to dephasing proportional to the bath temperature, $\Gamma_m = \gamma_n N_{\text{th}}^{(n)}$. A similar conclusion can be derived from a master-equation approach³⁸, which however does not treat low-frequency noise correctly and ignores the high-frequency 'cutoff' $v_n(\omega \gg \omega_n, t) \sim \omega^{-2}$.

Received 18 June 2009; accepted 21 April 2010; published online 30 May 2010

References

- Cirac, J. I. & Zoller, P. Quantum computations with cold trapped ions. *Phys. Rev. Lett.* **74**, 4091–4094 (1995).
- Leibfried, D. *et al.* Creation of a six-atom 'Schrödinger cat' state. *Nature* **438**, 639–642 (2005).
- Hänsel, W. *et al.* Scalable multiparticle entanglement of trapped ions. *Nature* **438**, 643–646 (2005).
- Maunz, P. *et al.* Entanglement of single-atom quantum bits at a distance. *Nature* **449**, 68–71 (2007).
- Jelezko, F. & Wrachtrup, J. Read-out of single spins by optical spectroscopy. *J. Phys. Condens. Matter* **16**, R1089–R1104 (2004).
- Jelezko, F. *et al.* Observation of coherent oscillation of a single nuclear spin and realization of a two-qubit conditional quantum gate. *Phys. Rev. Lett.* **93**, 130501 (2004).
- Hanson, R., Mendoza, F. M., Epstein, R. J. & Awschalom, D. D. Polarization and readout of coupled single spins in diamond. *Phys. Rev. Lett.* **97**, 087601 (2006).
- Childress, L. *et al.* Coherent dynamics of coupled electron and nuclear spin qubits in diamond. *Science* **314**, 281–285 (2006).
- Dutt, M. V. G. *et al.* Quantum register based on individual electronic and nuclear spin qubits in diamond. *Science* **316**, 1312–1316 (2007).
- Kane, B. E. A silicon-based nuclear spin quantum computer. *Nature* **393**, 133–137 (1998).
- Tyryshkin, A. M. *et al.* Solid-state quantum memory using the P nuclear spin. *Nature* **455**, 1085–1088 (2008).
- Tyryshkin, A. M., Lyon, S. A., Astashkin, A. V. & Raitsimring, A. M. Electron spin relaxation times of phosphorus donors in silicon. *Phys. Rev. B* **68**, 193207 (2003).
- Stegner, A. R. *et al.* Electrical detection of coherent 31P spin quantum states. *Nature Phys.* **2**, 835–838 (2006).
- Harneit, W. Fullerene-based electron-spin quantum computer. *Phys. Rev. A* **65**, 032322 (2002).
- Benjamin, S. C. *et al.* Towards a fullerene-based quantum computer. *J. Phys. Condens. Matter* **18**, S867–S883 (2006).
- Morton, J. J. L. *et al.* Bang–bang control of fullerene qubits using ultrafast phase gates. *Nature Phys.* **2**, 40–43 (2006).
- Churchill, H. O. H. *et al.* Relaxation and dephasing in a two-electron ¹³C nanotube double quantum dot. *Phys. Rev. Lett.* **102**, 166802 (2009).
- Trauzettel, B., Bulaev, D. V., Loss, D. & Burkard, G. Spin qubits in graphene quantum dots. *Nature Phys.* **3**, 192–196 (2007).
- Vrijen, R. *et al.* Electron–spin–resonance transistors for quantum computing in silicon–germanium heterostructures. *Phys. Rev. A* **62**, 012306 (2000).
- Zwanenburg, F. A., van Rijmenam, C. E. W. M., Fang, Y., Lieber, C. M. & Kouwenhoven, L. P. Spin states of the first four holes in a silicon nanowire quantum dot. *Nano Lett.* **9**, 1071–1079 (2009).
- Rugar, D., Budakian, R., Mamin, H. J. & Chui, B. W. Single spin detection by magnetic resonance force microscopy. *Nature* **430**, 329–332 (2004).
- Mamin, H. J. *et al.* Isotope-selective detection and imaging of organic nanolayers. *Nano Lett.* **9**, 3020–3024 (2009).
- Naik, A. *et al.* Cooling a nanomechanical resonator with quantum back-action. *Nature* **443**, 193–196 (2006).
- Gigan, S. *et al.* Self-cooling of a micro-mirror by radiation pressure. *Nature* **444**, 67–70 (2006).
- Schliesser, A., Riviere, R., Anetsberger, G., Arcizet, O. & Kippenberg, T. J. Resolved-sideband cooling of a micromechanical oscillator. *Nature Phys.* **4**, 415–419 (2008).
- Thompson, J. D. *et al.* Strong dispersive coupling of a high-finesse cavity to a micromechanical membrane. *Nature* **452**, 72–75 (2008).
- Teufel, J. D., Harlow, J. W., Regal, C. A. & Lehnert, K. W. Dynamical backaction of microwave fields on a nanomechanical oscillator. *Phys. Rev. Lett.* **101**, 197203 (2008).
- Rabl, P. *et al.* Strong magnetic coupling between an electronic spin qubit and a mechanical resonator. *Phys. Rev. B* **79**, 041302(R) (2009).
- Armour, A. D., Blencowe, M. P. & Schwab, K. C. Entanglement and decoherence of a micromechanical resonator via coupling to a Cooper-pair box. *Phys. Rev. Lett.* **88**, 148301 (2002).
- Treutlein, P., Hunger, D., Camerer, S., Hänsch, T. W. & Reichel, J. Bose–Einstein condensate coupled to a nanomechanical resonator on an atom chip. *Phys. Rev. Lett.* **99**, 140403 (2007).
- Tian, L. & Zoller, P. Coupled ion–nanomechanical systems. *Phys. Rev. Lett.* **93**, 266403 (2004).
- Hensinger, W. K. *et al.* Ion trap transducers for quantum electromechanical oscillators. *Phys. Rev. A* **72**, 041405 (2005).
- Balazsramanian, G. *et al.* Ultralong spin coherence time in isotopically engineered diamond. *Nature Mater.* **8**, 383–387 (2009).
- Sorensen, A. & Molmer, K. Quantum computation with ions in thermal motion. *Phys. Rev. Lett.* **82**, 1971–1974 (1999).
- Molmer, K. & Sorensen, A. Multiparticle entanglement of hot trapped ions. *Phys. Rev. Lett.* **82**, 1835–1838 (1999).
- Wunderlich, C., Figger, H., Meschede, D. & Zimmermann, C. *Laser Physics at the Limit* (Springer, 2002).
- Garca-Ripoll, J. J., Zoller, P. & Cirac, J. I. Speed optimized two-qubit gates with laser coherent control techniques for ion trap quantum computing. *Phys. Rev. Lett.* **91**, 157901 (2003).
- Garca-Ripoll, J. J., Zoller, P. & Cirac, J. I. Coherent control of trapped ions using off-resonant lasers. *Phys. Rev. A* **71**, 062309 (2005).
- Leggett, A. J. *et al.* Dynamics of the dissipative two-state system. *Rev. Mod. Phys.* **59**, 1–85 (1987).
- Kitagawa, M. & Ueda, M. Squeezed spin states. *Phys. Rev. A* **47**, 5138–5143 (1993).
- Dür, W. & Briegel, H. J. Entanglement purification for quantum computation. *Phys. Rev. Lett.* **90**, 067901 (2003).
- Jiang, L., Taylor, J. M., Sorensen, A. S. & Lukin, M. D. Distributed quantum computation based on small quantum registers. *Phys. Rev. A* **76**, 062323 (2007).
- de Sousa, R. & Das Sarma, S. Theory of nuclear-induced spectral diffusion: Spin decoherence of phosphorus donors in Si and GaAs quantum dots. *Phys. Rev. B* **68**, 115322 (2003).
- Coish, W. A. & Loss, D. Hyperfine interaction in a quantum dot: Non-Markovian electron spin dynamics. *Phys. Rev. B* **70**, 195340 (2004).
- Maze, J. R., Taylor, J. M. & Lukin, M. D. Electron spin decoherence of single nitrogen-vacancy defects in diamond. *Phys. Rev. B* **78**, 094303 (2008).
- Zimmerli, G., Eiles, T. M., Kautz, R. L. & Martinis, J. M. Noise in the Coulomb blockade electrometer. *Appl. Phys. Lett.* **61**, 237–239 (1992).
- Haeberlen, U. *High Resolution NMR in Solids: Selective Averaging* (Academic, 1976).
- Uhrig, G. S. Keeping a quantum bit alive by optimized π -pulse sequences. *Phys. Rev. Lett.* **98**, 100504 (2007).
- Raussendorf, R. & Briegel, H. J. A one-way quantum computer. *Phys. Rev. Lett.* **86**, 5188–5191 (2001).
- Garg, A., Onuchic, J. N. & Ambegaokar, V. Effect of friction on electron transfer in biomolecules. *J. Chem. Phys.* **83**, 4491–4503 (1985).

Acknowledgements

We gratefully acknowledge discussion with M. Aspelmeyer and K. Schwab. This work is supported by ITAMP, NSF, CUA, DARPA and the Packard Foundation. P.Z. acknowledges support by SFB FOQUS and EU Networks.

Author contributions

P.R. carried out the theoretical analysis of the coupling scheme. All authors contributed to the initial ideas, discussions of the results and writing the manuscript.

Additional information

The authors declare no competing financial interests. Supplementary information accompanies this paper on www.nature.com/naturephysics. Reprints and permissions information is available online at <http://npg.nature.com/reprintsandpermissions>. Correspondence and requests for materials should be addressed to P.R.